

Correlated structural and electronic phase transformations in transition metal chalcogenide under high pressure

Chunyu Li, Feng Ke, Qingyang Hu, Zhenhai Yu, Jinggeng Zhao, Zhiqiang Chen, and Hao Yan

Citation: [Journal of Applied Physics](#) **119**, 135901 (2016); doi: 10.1063/1.4945323

View online: <http://dx.doi.org/10.1063/1.4945323>

View Table of Contents: <http://scitation.aip.org/content/aip/journal/jap/119/13?ver=pdfcov>

Published by the [AIP Publishing](#)

Articles you may be interested in

[Semiconductor-to-metal transition of Bi₂Se₃ under high pressure](#)

Appl. Phys. Lett. **105**, 062102 (2014); 10.1063/1.4892661

[Electronic topological transition and semiconductor-to-metal conversion of Bi₂Te₃ under high pressure](#)

Appl. Phys. Lett. **103**, 052102 (2013); 10.1063/1.4816758

[First-principles study of pressure-induced phase transition and electronic property of PbCrO₃](#)

J. Appl. Phys. **111**, 013503 (2012); 10.1063/1.3673865

[Phase transition of Zn₂SnO₄ nanowires under high pressure](#)

J. Appl. Phys. **106**, 113523 (2009); 10.1063/1.3268460

[Effect of alkaline-earth and transition metals on the electrical transport of double perovskites](#)

J. Appl. Phys. **95**, 6261 (2004); 10.1063/1.1728294

A promotional banner for AIP Applied Physics Reviews. The background is a dark blue gradient with a bright light source on the right, creating a lens flare effect. On the left, there is a small image of the journal cover for 'Applied Physics Reviews', which features a 3D diagram of a layered material structure. The main text 'NEW Special Topic Sections' is written in large, white, sans-serif font. Below this, the text 'NOW ONLINE' is in yellow, followed by 'Lithium Niobate Properties and Applications: Reviews of Emerging Trends' in white. The AIP Applied Physics Reviews logo is in the bottom right corner.

NEW Special Topic Sections

NOW ONLINE
Lithium Niobate Properties and Applications:
Reviews of Emerging Trends

AIP Applied Physics
Reviews

Correlated structural and electronic phase transformations in transition metal chalcogenide under high pressure

HPSTAR
2016-191

Chunyu Li,^{1,a)} Feng Ke,¹ Qingyang Hu,^{1,2} Zhenhai Yu,¹ Jinggeng Zhao,³ Zhiqiang Chen,¹ and Hao Yan^{1,a)}

¹Center for High Pressure Science and Technology Advanced Research, Shanghai 201203, People's Republic of China

²Geophysical Laboratory, Carnegie Institution of Washington, Washington, DC 20015, USA

³Natural Science Research Center, Academy of Fundamental and Interdisciplinary Sciences, Harbin Institute of Technology, Harbin 150080, People's Republic of China

(Received 25 December 2015; accepted 22 March 2016; published online 4 April 2016)

Here, we report comprehensive studies on the high-pressure structural and electrical transport properties of the layered transition metal chalcogenide (Cr_2S_3) up to 36.3 GPa. A structural phase transition was observed in the rhombohedral Cr_2S_3 near 16.5 GPa by the synchrotron angle dispersive X-ray diffraction measurement using a diamond anvil cell. Through *in situ* resistance measurement, the electric resistance value was detected to decrease by an order of three over the pressure range of 7–15 GPa coincided with the structural phase transition. Measurements on the temperature dependence of resistivity indicate that it is a semiconductor-to-metal transition in nature. The results were also confirmed by the electronic energy band calculations. Above results may shed a light on optimizing the performance of Cr_2S_3 based applications under extreme conditions. © 2016 AIP Publishing LLC. [<http://dx.doi.org/10.1063/1.4945323>]

I. INTRODUCTION

Layered transition metal chalcogenides play an important role in thermoelectric applications. For example, they are functional components in refrigeration, heat pumping, and power generation.^{1–4} Within the A_2X_3 -type chalcogenides ($\text{A} = \text{Cr}, \text{Bi}, \text{As}, \text{Sb}, \text{Sn}$ and $\text{X} = \text{O}, \text{S}, \text{Se}, \text{Te}$), Cr_2S_3 stands out for its interesting novel physical properties, such as ferromagnetic, semi-conducting, and thermoelectric properties presented under some conditions.⁵ The electrical and magnetic properties of Cr_2S_3 can be controlled by varying temperatures and stoichiometries.⁶ It is also suggested that the rhombohedral phase Cr_2S_3 is a semiconductor, and both n-type and p-type conductivity can be realized by different sample preparation methods.⁷ Previously, a study on its magnetic properties observed linear increase of Curie temperature with pressure.^{8,9} Mechanism-wise, the magnetic and electrical properties were governed by the Cr atom vacancies in the metal layers, which is also tuned by temperature and pressure.¹⁰ It suggests that the magnetization stems from the layered structure of Cr_2S_3 , that is highly depending on the external pressure. So the information on the structure of Cr_2S_3 under high pressure is valuable for further physical property studies. It is of interest that the crystal structure of Cr_2S_3 is similar with the very popular thermoelectric materials $\text{Bi}_2(\text{Se}, \text{Te})_3$ and $(\text{Bi}, \text{Sb})_2\text{Te}_3$, which were found as topological insulators recently owning the crystal polymorphisms under different external conditions.

Despite the broad interest on Cr_2S_3 , few previous experimental and theoretical results can be referred on the structural and electrical transportation information under high

pressure. Most structure studies under high pressure have been devoted to A_2X_3 -type transition metal sesquioxides compared to chalcogenides,^{11–18} due to their vital application in the process of ceramics as additives, grain growth inhibitors, and phase stabilizers.¹⁹ Cr_2O_3 , which is isoelectronic with Cr_2S_3 , was found absent of structural phase transition to 10 GPa (Refs. 20 and 21) using powder and single-crystal X-ray diffraction (XRD) techniques.²² However, similar to the distortion occurring in V_2O_3 at low temperature, Cr_2O_3 was observed undergoing a phase transition to a monoclinic structure under high pressure.^{23–26} Cr_2S_3 is rather peculiar as it exists in two crystallographic forms, trigonal and rhombohedral at ambient conditions.²⁷ To further explore the high-pressure structural evolution and its correlation with the electrical transport properties of Cr_2S_3 , the high-pressure structural evolution of Cr_2S_3 was investigated using *in situ* synchrotron XRD techniques combined with diamond anvil cell (DAC). And the high-pressure electrical transport properties were also detected by the high-pressure resistance measurement. Furthermore, first-principle calculations were performed to reproduce our experimental results.

II. EXPERIMENTAL AND THEORETICAL DETAILS

A. Angular dispersive X-ray diffraction (AD-XRD) experiments

In this work, Cr_2S_3 sample was purchased from Alfa Aesar's company with 99% purity. The sample was examined by powder AD-XRD and found in a single phase with the lattice constants $a = 5.9370$ and $c = 16.6980$ Å. The high-pressure powder AD-XRD patterns were collected using a focused synchrotron beam at the X17C beamline of the National Synchrotron Light Source (NSLS), Brookhaven National Laboratory (BNL). During experiment, the

^{a)}Authors to whom correspondence should be addressed. Electronic addresses: licy@hpstar.ac.cn and yanhao@hpstar.ac.cn.

monochromatic beam has a wavelength of 0.4075 Å. Symmetric DAC with a diamond culet size of 300 μm was used to apply pressure. Pre-compressed pellets were loaded into a 120 μm diameter sample chamber of pre-indented stainless gasket made of 45 μm in thickness a symmetric DAC. Silicone oil was used as a pressure transmitting medium. The pressure was calibrated by ruby fluorescence. The XRD patterns at various pressures were collected using an online CCD detector with a 165 mm diameter active area (size of horizontal/vertical pixels: 79.59 μm). The two-dimensional diffraction rings were integrated into the one-dimensional XRD patterns using the FIT2D program.²⁸ The XRD patterns of the low-pressure (LP) phase Cr₂S₃ were analyzed with Rietveld refinement using the GSAS program package²⁹ with the user interface EXPGUI.³⁰ An independent angle dispersive XRD study of Cr₂S₃ under high pressure was also carried out at the BL15U1 beamline of the Shanghai Synchrotron Radiation Facility (SSRF) using a wavelength of 0.6199 Å and a CCD detector with a 165 mm diameter active area (size of horizontal/vertical pixels: 79.59 μm).

B. *In-situ* resistance measurement

The high-pressure electrical resistance measurement for Cr₂S₃ was performed using a four-electrode method without pressure transmitting medium. Four electrodes were set up on one side of the diamond anvil. And a gasket was put on the other side, on which a smaller hole of 150 μm in diameter was drilled to serve as the sample chamber. To build insulation to the electrodes, the hole in the gasket was filled in by compacted c-BN powder, and the rest part of the gasket was covered by the insulating gel. The resistance measuring DAC was checked by ohmmeter to make sure that it works well before taking measurement. The high-temperature high-pressure resistance measurement for Cr₂S₃ was conducted on a temperature-controlled hot plate.

C. First principles calculations

First-principle calculations³¹ were performed in the framework of density functional theory by the Vienna *Ab initio* Simulation Package (VASP).³² The generalized gradient approximation (GGA) parametrized by Perdew-Burke-Ernzerhof (PBE)³³ with the Hubbard *U* method³⁴ is implemented to describe the exchange correlation function. The value of *U* (3.2 eV) in this work is determined by the linear reposed method. The projected-augmented wave potentials are used with 6 valence electrons for Cr ($3d^5 4s^1$) and 6 for S ($2s^2 2p^4$). A plane-wave basis set with a kinetic energy cut off of 400 eV is found sufficient to converge the total energy less than 10⁻⁶ eV and force acting on each atom less than 0.01 eV/Å, where the Brillouin zone is sampled by a Monkhorst mesh of 8 × 8 × 2 k-points. Spin polarized calculation with ferromagnetic magnetic ordering³⁵ is initialized for the rhombohedral Cr₂S₃ phase. Hydrostatic pressure is applied by adding Pulay stress to the diagonal elements of the stress tensor. At each pressure, the unit cell is fully optimized for atomic position, cell shape, and cell volume.

We carried out phonon analysis to confirm the mechanical stability of Cr₂S₃ under pressure. The calculation is implemented by the finite displacement method within the Phonopy package.³⁶ Force constants are calculated using the Moore–Penrose pseudo-inverse by fitting symmetry reduced elements of force constants to the linear relations between atomic forces and atomic displacements. The detailed calculation results will be shown in Sec. III.

III. RESULTS AND DISCUSSION

The crystal structure of the chromium sulfides at room temperature has been detected by Jelinek.²⁷ Cr₂S₃ can crystallize into two different crystal structures due to a small deviation from stoichiometric composition Cr₂S₃. The trigonal phase of Cr₂S₃ can be formed by reacting at high temperature under pressure (short for spark plasma sintering (SPS) process) starting from the powder of the rhombohedral phase Cr₂S₃ precursor.³⁷ The two different structures of Cr₂S₃ could be described as intermediate between the NiAs and Cd(OH)₂ types. To illuminate the differences and correlation of the trigonal/rhombohedral Cr₂S₃, the detailed structural informations for them are in Table I. And a schematic representation is shown in Fig. S1 (see supplementary material³⁸ for details). Both the trigonal and the rhombohedral phases of Cr₂S₃ have an ordered atom arrangement in the planes perpendicular to the (001) directions. The S atoms are packed hexagonally to form the octahedral voids which are fully or unfully occupied by the metal atoms Cr to form the alternate “CrS” and “Cr_{1/3}S” stacking layers. The two phases differ only by the arrangement of the unfully occupied Cr vacancies.

The phase transitions from one crystal structure to another by change of temperature, chemical position, or pressure are one of the most fundamental research topics in geoscience, physics, and material. In order to clarify the potential structural changes at high pressure, the *in situ* high-pressure powder AD-XRD experiment for the rhombohedral phase of Cr₂S₃ was carried out at room temperature with a stepwise pressure increasing up to 32.5 GPa. The selected AD-XRD patterns are demonstrated in Fig. 1 with a small amount of impurity

TABLE I. The detailed structural informations for trigonal and rhombohedral phases of Cr₂S₃.

	Space group	Lattice parameters	Wyckoff positions
Cr ₂ S ₃ (trigonal)	<i>P</i> -31 <i>c</i>	$a = 5.939(2) \text{ \AA}^a$ $c = 11.192(3) \text{ \AA}^a$	Cr(1), 2(c): $\pm(1/3, 2/3, 1/4)$ Cr(2), 2(b): (0, 0, 0); (0, 0, 1/2) Cr(3), 4(f): $\pm(1/3, 2/3, z)$; $\pm(1/3, 2/3, 1/2-z)$ S, 12(i): $\pm(x, y, z)$
Cr ₂ S ₃ (rhombohedral)	<i>R</i> -3	$a = 5.937(2) \text{ \AA}^a$ $c = 16.698(5) \text{ \AA}^a$ $a = 5.949(3) \text{ \AA}^b$ $c = 16.727(2) \text{ \AA}^b$	Cr(1), 3(b): (0, 0, 1/2) Cr(2), 3(a): (0, 0, 0) Cr(3), 6(c): $\pm(0, 0, z)$ S, 18(f): $\pm(x, y, z)$ (in hexagonal description)

^aRepresent the result from Ref. 27.

^bRepresent the result from our experiments.

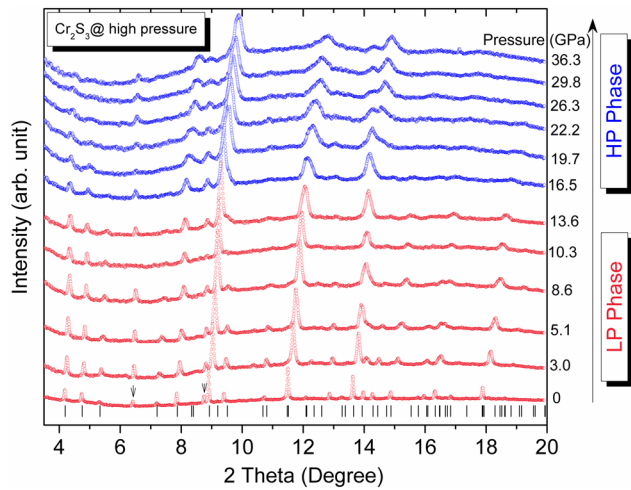


FIG. 1. Angle dispersive X-ray diffraction patterns of Cr_2S_3 under various pressures up to 36.3 GPa at room temperature ($\lambda = 0.4075 \text{ \AA}$, experiment conducted at X17C).

marked with down arrow. It can be seen that all the diffraction peaks broaden as the pressure increases, which were caused by the pressure gradient in the sample chamber (silicone oil is not quasi-hydrostatic beyond 6 GPa)^{39–41} and sample thinning. All the diffraction peaks for Cr_2S_3 shift to the higher angle with increasing pressure, indicating the shrinking of lattices. Some new diffraction peaks appear at 16.5 GPa in the AD-XRD patterns of Cr_2S_3 showed in Fig. 1, suggesting the occurrence of a pressure-induced structural phase transition at about 16.5 GPa. The structure of the high-pressure phase needs further identification. The diffraction peaks could be still indexed by the ambient rhombohedral phase after the pressure was released to 0 GPa (the pressure was released step by step (not quenched)) as shown in Fig. S2 (see supplementary material³⁸ for details), indicating that this structural phase transition in Cr_2S_3 is reversible. The experimental results obtained at BL15U1 at SSRF were consistent with that collected at X17C beamline at BNL shown in Fig. S3 (see supplementary material³⁸ for details).

All pressure-induced phase transitions have some common features. One common rule is that the atomic arrangements in the compounds containing light elements at high pressures will become to those observed in analogous compounds containing heavy elements at lower pressures, which is so-called “corresponding static principle.”⁴² Such as, the elements Cr, Mo, and W all belong to the same main group. Mo_2S_3 have been reported having a monoclinic structure at ambient conditions.⁴³ It is naturally to assume that Cr_2S_3 could adopt a monoclinic phase under high pressure. And the GdFeO_3 -type structure (Space group: $Pnma$, with $Z = 4$) is also one of the possible high pressure phase of Cr_2S_3 .⁴⁴ Furthermore, it can be seen from the XRD patterns of Cr_2S_3 , the original diffraction peaks did not disappear except the intensity changing and some new diffraction peaks showing up. So this should be a second-order phase transition. We searched for the possible crystal structure models to index the high-pressure phase diffractogram by referring to the known A_2X_3 -type metal sulfides. While the exploring for the high-pressure phase is still not successful.

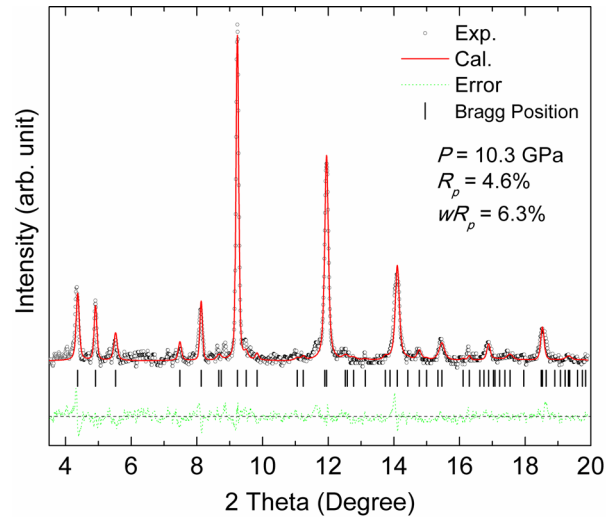


FIG. 2. Typical Rietveld refinement of the LP phase of Cr_2S_3 at 10.3 GPa ($\lambda = 0.4075 \text{ \AA}$). The vertical bars represent the calculated positions of the diffraction peaks of Cr_2S_3 . The difference between the observed (circles) and the fitted patterns (line) is shown with a green line at the bottom of the diffraction peaks.

The structural parameters of the LP phase of Cr_2S_3 can be obtained by Rietveld refinement of the AD-XRD patterns. A typical Rietveld refinement result of the XRD pattern for the LP phase of Cr_2S_3 at 10.3 GPa is shown in Fig. 2. The atomic coordinates of the Cr and S atoms were not included in the Rietveld refinement. The vertical bars represent the calculated position of the diffraction peaks of Cr_2S_3 . The difference between the observed (circles) and the fitted patterns (line) is shown with a dotted green line at the bottom of the diffraction peaks.

The pressure dependence of the lattice parameters for the LP phase of Cr_2S_3 is shown in Fig. 3(b). The lattice parameters homogeneously decrease as the pressure increases for the LP phase of Cr_2S_3 . The pressure dependence of the axial relative compressibilities c/c_0 and a/a_0 for the LP phase of Cr_2S_3 is shown in Fig. 3(a). The relative compressibility

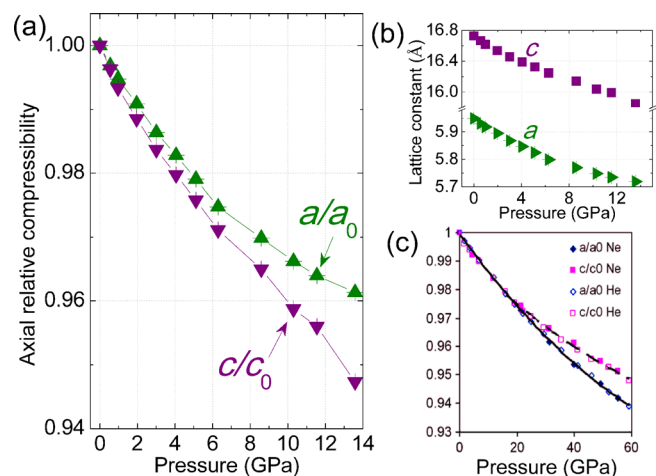


FIG. 3. (a) The pressure evolution of the axial relative compressibilities for LP phase of Cr_2S_3 . (b) The pressure dependence of the lattice parameters of the LP phase of Cr_2S_3 . (c) The pressure dependence of the axial relative compressibilities for Cr_2O_3 , which was taken from Ref. 22.

of the c -axis is a little larger than that of the a -axis, that is, the interlayer distance (c -axis) decreases more significantly than the intralayer distance (a -axis). This anisotropy is relevant to the crystallographic stacking characteristic of Cr_2S_3 and indicates that the bonding along the a -axis is a little weaker than that of the c -axis. Compared to the results of Cr_2O_3 from Ref. 22 shown in Fig. 3(c), the changing trend of the high-pressure compressibilities in Cr_2S_3 is totally different from those of Cr_2O_3 . The axial relative compressibilities of Cr_2O_3 are almost same below 15 GPa and then show an anisotropy with further pressure increasing.

Fig. 4 shows the volume–pressure data for the LP phase of Cr_2S_3 , which are fitted to a three-order Birch–Murnaghan equation of state (EOS).⁴⁵ The EOS parameters V_0 (unit cell volume at ambient pressure), B_0 (isothermal bulk modulus), and B_0' (pressure derivative of B_0) are yielded as $V_0 = 511.41(9) \text{ \AA}^3$, $B_0 = 59.8(6) \text{ GPa}$, and $B_0' = 9.1$ by least-square fitting.⁴⁶

Under high pressure, a structural or iso-structural phase transition is often accompanied by an electronic phase transition. The distance decreasing of the atoms in the intra- as well as interlayers of Cr_2S_3 is expected to alter the electronic properties, which can be reflected by the electronic transport property measurement. The resistance–pressure relation measured for Cr_2S_3 was plotted in Fig. 5. It can be seen from Fig. 5(a) that both the resistances R_{14} and R_{34} appear a gradual decrease first, and then a much steeper decrease of about three orders of magnitude is observed during the pressure range of 6–15 GPa. Finally, the slope becomes a little gentle above the pressure point of 15 GPa, and the resistance almost saturates to their minimum values up to around 21.5 GPa. By reacting at high temperature under pressure (SPS process), the authors in Ref. 36 obtained the trigonal phase of Cr_2S_3 , which can be seen as the high-pressure high-temperature phase of Cr_2S_3 . It is remarkable to note that the resistivity of the trigonal phase of Cr_2S_3 (Ref. 37) shows a large decrease (more than one order magnitude) compared with that of the rhombohedral phase. This phenomenon is similar with the resistivity changing of Cr_2S_3 under high pressure in our present work. It should be noticed that the values of R_{14} and R_{34} are not the same due to the unsymmetric distribution of the four electrodes on the sample surface, which will not affect

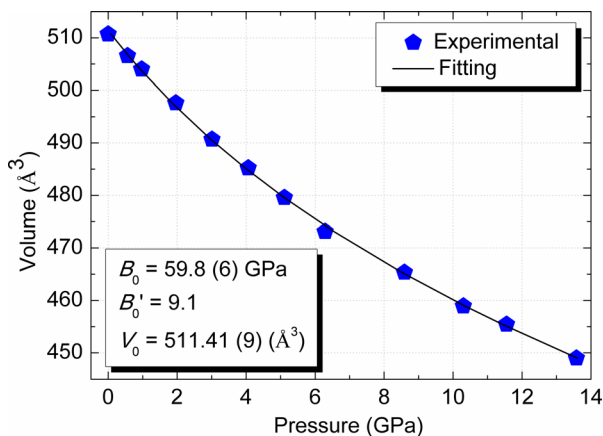


FIG. 4. The experimental pressure dependence of the Cr_2S_3 unit cell volume fitted by a 3rd order Birch–Murnaghan equation of state.

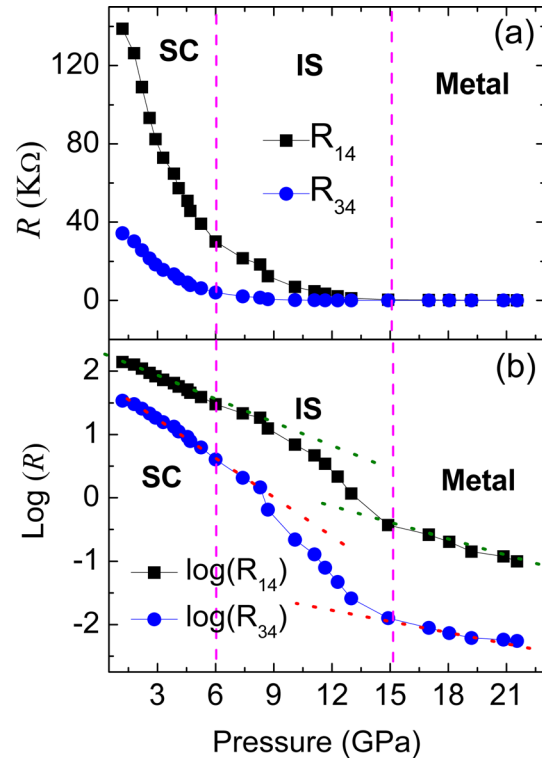


FIG. 5. The pressure dependence of the electrical resistances for Cr_2S_3 . (a) R_{14} and R_{34} , (b) $\text{Log}(R_{14})$ and $\text{Log}(R_{34})$ (the dotted lines are for the eyes' guide).

the accuracy of the measurement results. To discern the novel change of the electrical resistance more clearly, the corresponding $\log(R)$ – P relations are plotted in Fig. 5(b). The semiconductor Cr_2S_3 has become metallic from semiconductive under high pressure. We can label these different regions as the semiconducting (SC), intermediate state (IS), and metallic regions, respectively, as shown in Fig. 5. It suggests that the electronic density of state at the Fermi surface of Cr_2S_3 has been turned, and the band gap is effectively reduced by compression. The similar phenomenon was also found in p-type semiconductor ribbon-like Bi_2S_3 studied by Zahedi using density functional theory (DFT) methods.¹⁸

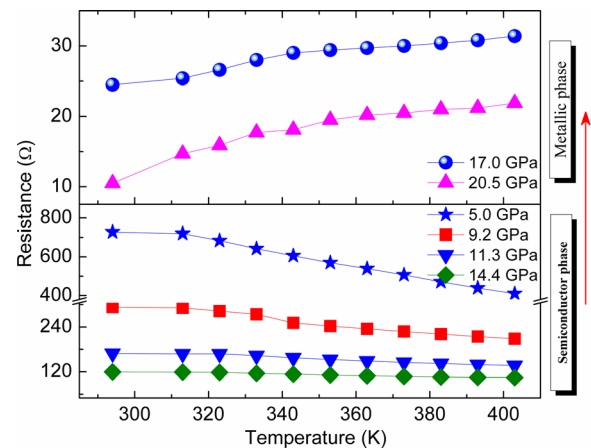


FIG. 6. The temperature dependence of the electrical resistance in Cr_2S_3 under various pressures up to 20.5 GPa. (The pressure-induced semiconductor \rightarrow metal transition is characterized by contrasting the temperature dependence of resistance under different pressures.)

To determine whether or not Cr_2S_3 undergoes a semiconductor–metal transformation under high pressure, the temperature dependence of the resistance was also measured for Cr_2S_3 between 300 and 400 K at several representative pressures (shown in Fig. 6). It can be seen that the temperature coefficients of Cr_2S_3 are negative ($dR/dT < 0$) below the pressure of 14.4 GPa, indicating that Cr_2S_3 has the semiconductor behavior, and the absolute value of dR/dT decreases as the pressure increases up to 14.4 GPa. It is remarkable to note that the resistance of Cr_2S_3 starts to increase as the temperature further increases; that is, the temperature coefficients of Cr_2S_3 become positive ($dR/dT > 0$) above 17 GPa, indicating that Cr_2S_3 has a semiconductor–metal transformation under high pressure. There was no pressure transmitting

medium used in the high pressure resistance measurement. Therefore, the transition pressure derived from the resistance and XRD measurements shows different values, since the high pressure XRD measurement was used silicone oil as the pressure transmitting medium and the deviatoric stresses could result into strong influence on physical properties' measurement.⁴⁷

To understand the electronic properties and illuminate the underlying physics reasoning for the resistance–pressure relation in the rhombohedral Cr_2S_3 , the high-pressure electronic band structures are evaluated by first-principle calculations. The energy bands at 0, 15, and 30 GPa are shown in Fig. 7, respectively. Because of the ferrimagnetic nature of the rhombohedral Cr_2S_3 , the spin-up energy band and spin-

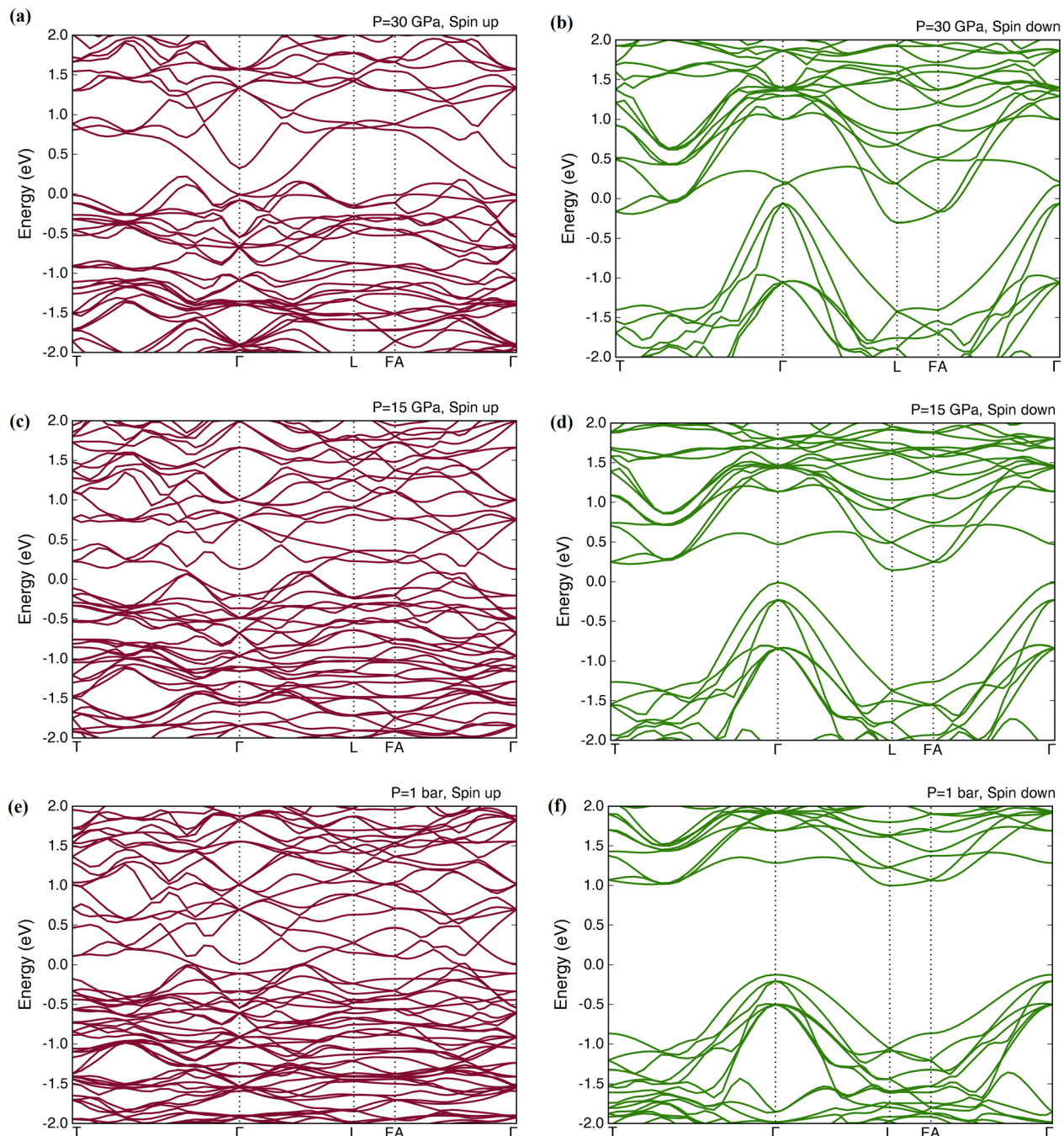


FIG. 7. The experimental high pressure spin-up energy bands and spin-down energy bands of Cr_2S_3 at 0, 15, and 30 GPa by first principal calculations.

down energy bands are asymmetric. It can be seen that Cr_2S_3 is an indirect semiconductor at 0 GPa. With the pressure increasing, the valence band maxima (VBM) at the Γ point and the conduction band minima (CBM) at the L point start to move toward the Fermi level, which makes the E_g reduces further. The VBM and the CBM almost touch the Fermi level at a pressure of 15 GPa for the spin-down energy band of Cr_2S_3 (Fig. 7), and the rhombohedral Cr_2S_3 becomes metallic when the pressure increases up to 30 GPa, which correlates well with the transition pressures in the experimental XRD and resistivity measurements of Cr_2S_3 . Due to no transmission medium for the resistance measurement, the onset of the novel electron change appears under relative lower pressure than that for the crystal structure phase transition by XRD measurement. It means high pressure has changed the electrical structure of the rhombohedral Cr_2S_3 .

The effect of pressure on the vibrational properties of Cr_2S_3 can be understood using theoretically calculated phonon dispersion curves. The calculated phonon spectrums for the LP phase of Cr_2S_3 were shown in Fig. S4 (see supplementary material³⁸ for details). It can be seen that from T to Γ point, the optical modes with the lowest frequencies have presented pressure-induced softening to a certain extent in the rhombohedral Cr_2S_3 around the phase transition point 15 GPa, which may contribute to the high pressure crystal structural and electronic phase transitions in Cr_2S_3 . Several materials have been previously reported to exhibit an intermediate state with soften phonon behavior while undergoing a transition from a semiconductor to a metallic state.^{48,49} And the similar optical modes' softening has also occurred for some ferroelectric materials accompanying with the displacement-type second-order phase transitions.⁵⁰

IV. CONCLUSION

To summarize, we have found a structural phase transition in the rhombohedral Cr_2S_3 at about 16.5 GPa through the *in situ* high pressure AD-XRD experiments. The new phase is reversible during decompression. The compressibility of the LP phase of Cr_2S_3 is anisotropic. The electric resistance measurement shows that the resistance decreased by three magnitudes after phase transition. The high-temperature high-pressure electrical resistance measurement indicates that Cr_2S_3 experiences a semiconductor-to-metal transition under high pressure. And our energy band structure calculation results agree well with above conclusion. The phonon spectrum calculations show the mode softening around the phase transition pressure 15 GPa. The high-pressure structural phase transition may be accompanied by a magnetic phase transition in Cr_2S_3 , which needs to be confirmed in the future research.

ACKNOWLEDGMENTS

We acknowledge the National Synchrotron Light Source (NSLS) of Brookhaven National Laboratory (BNL) for the provision of synchrotron radiation facilities beam line X17C. We are thankful for the support from COMPRES (the Consortium for Materials Properties Research in Earth Sciences). Portions of this work were performed at the BL15U1 beamline, Shanghai Synchrotron Radiation Facility

in China. The authors would like to thank Shanghai Synchrotron Radiation Source for use of the synchrotron radiation facilities. This work was partially supported by the Natural Science Foundation of China (Grant No. 10904022). The computational work was conducted on the SR10000-K1/52 supercomputing facilities of the Institute for Materials Research, Tohoku University. We are grateful to the editor and anonymous referees for their thorough reading of the paper and suggestion for improvement.

- ¹H. J. Zhang, C. X. Liu, X. L. Qi, X. Dai, Z. Fang, and S. C. Zhang, *Nat. Phys.* **5**, 438 (2009).
- ²Y. L. Chen, J. G. Analytis, J.-H. Chu, Z. K. Liu, S.-K. Mo, X. L. Qi, H. J. Zhang, D. H. Lu, X. Dai, Z. Fang, S. C. Zhang, I. R. Fisher, Z. Hussain, and Z.-X. Shen, *Science* **325**, 178 (2009).
- ³G. J. Snyder and E. S. Tjebke, *Nat. Mater.* **7**, 105 (2008).
- ⁴L. E. Bell, *Science* **321**, 1457 (2008).
- ⁵C. F. van Bruggen, M. B. Vellinga, and C. Haas, *J. Solid State Chem.* **2**, 303 (1970).
- ⁶M. Mikami, K. Igaki, and N. Ōhashi, *J. Phys. Soc. Jpn.* **32**, 1217 (1972).
- ⁷K. R. Pisharody, *J. Solid State Chem.* **30**, 149 (1979).
- ⁸M. Yuzuri and T. Yusuiki, *J. Magn. Magn. Mater.* **54–57**, 923 (1986).
- ⁹M. Yuzuri, T. Kanomata, and T. Kaneko, *J. Magn. Magn. Mater.* **70**, 223 (1987).
- ¹⁰M. Yuzuri and Y. Nakamura, *J. Phys. Soc. Jpn.* **19**, 1350 (1964).
- ¹¹O. Gomis, D. Santamaría-Pérez, J. Ruiz-Fuertes, J. A. Sans, R. Vilaplana, H. M. Ortiz, B. García-Domene, F. J. Manjón, D. Errandonea, P. Rodríguez-Hernández, A. Muñoz, and M. Mollar, *J. Appl. Phys.* **116**, 133521 (2014).
- ¹²B. García-Domene, J. A. Sans, O. Gomis, F. J. Manjón, H. M. Ortiz, D. Errandonea, D. Santamaría-Pérez, D. Martínez-García, R. Vilaplana, A. L. J. Pereira, A. Morales-García, P. Rodríguez-Hernández, A. Muñoz, C. Popescu, and A. Segura, *J. Phys. Chem. C* **118**, 20545 (2014).
- ¹³S. V. Ovsyannikov, E. Bykova, M. Bykov, M. D. Wenz, A. S. Pakhomova, K. Glazyrin, H.-P. Liermann, and L. Dubrovinsky, *J. Appl. Phys.* **118**, 165901 (2015).
- ¹⁴A. L. J. Pereira, D. Errandonea, A. Beltrán, L. Gracia, O. Gomis, J. A. Sans, B. García-Domene, A. Miquel-Veyrat, F. J. Manjón, A. Muñoz, and C. Popescu, *J. Phys.: Condens. Matter* **25**, 475402 (2013).
- ¹⁵Z. Zhao, Q. S. Zeng, H. J. Zhang, S. B. Wang, S. Hirai, Z. D. Zeng, and W. L. Mao, *Phys. Rev. B* **91**, 184112 (2015).
- ¹⁶B. García-Domene, H. M. Ortiz, O. Gomis, J. A. Sans, F. J. Manjón, A. Muñoz, P. Rodríguez-Hernández, S. N. Achary, D. Errandonea, D. Martínez-García, A. H. Romero, A. Singhal, and A. K. Tyagi, *J. Appl. Phys.* **112**, 123511 (2012).
- ¹⁷A. L. J. Pereira, L. Gracia, D. Santamaría-Pérez, R. Vilaplana, F. J. Manjón, D. Errandonea, M. Nalin, and A. Beltrán, *Phys. Rev. B* **85**, 174108 (2012).
- ¹⁸E. Zahedi, *Superlattices Microstruct.* **81**, 49 (2015).
- ¹⁹J. F. Lin, O. Degtyareva, C. T. Prewitt, P. Dera, N. Sata, E. Gregoryanz, H. K. Mao, and R. J. Hemley, *Nature Mater.* **3**, 389 (2004).
- ²⁰S. Rekhi, L. S. Dubrovinsky, R. Ahuja, S. K. Saxena, and B. Johansson, *J. Alloys Compd.* **302**, 16 (2000).
- ²¹J. Mougin, T. L. Bihan, and G. Lucazeau, *J. Phys. Chem. Solids* **62**, 553 (2001).
- ²²P. Dera, B. Lavina, Y. Meng, and V. B. Parkapenka, *J. Solid State Chem.* **184**, 3040 (2011).
- ²³S.-H. Shim, T. S. Duffy, R. Jeanloz, C.-S. Yoo, and V. Iota, *Phys. Rev. B* **69**, 144107 (2004).
- ²⁴P. D. Dernier and M. Marezio, *Phys. Rev. B* **2**, 3771 (1970).
- ²⁵D. B. McWhan and J. P. Remeika, *Phys. Rev. B* **2**, 3734 (1970).
- ²⁶C. Tenailleau, E. Suard, J. Rodriguez-Carvajal, A. Gibaud, and P. Lacorre, *J. Solid State Chem.* **174**, 431 (2003).
- ²⁷F. Jellinek, *Acta Crystallogr.* **10**, 620 (1957).
- ²⁸A. P. Hammersley, S. O. Svensson, M. Hanfland, A. N. Fitch, and D. Hausermann, *High Pressure Res.* **14**, 235 (1996).
- ²⁹A. C. Larson and R. B. Von Dreele, "General Structure Analysis System (GSAS)," Los Alamos National Laboratory Report LAUR 86-748 (1994).
- ³⁰B. H. Toby, *J. Appl. Cryst.* **34**, 210 (2001).
- ³¹X. Gonze, *Phys. Rev. B* **55**, 10337 (1997).
- ³²G. Kresse and J. Furthmüller, *Phys. Rev. B* **54**, 11169 (1996).

- ³³J. P. Perdew, K. Burke, and M. Ernzerhof, *Phys. Rev. Lett.* **77**, 3865 (1996).
- ³⁴V. I. Anisimov, J. Zaanen, and O. K. Andersen, *Phys. Rev. B* **44**, 943 (1991).
- ³⁵A. Maignan, E. Guilmeau, F. Cascoin, Y. Bréard, and V. Hardy, *Sci. Technol. Adv. Mater.* **13**, 053003 (2012).
- ³⁶A. Togo and I. Tanaka, *Scr. Mater.* **108**, 1 (2015).
- ³⁷A. Maignan, Y. Bréard, E. Guilmeau, and F. Gascoin, *J. Appl. Phys.* **112**, 013716 (2012).
- ³⁸See supplementary material at <http://dx.doi.org/10.1063/1.4945323> for detailed HP-XRD of Cr₂S₃ at BL15U1 and high pressure phonon spectrum of Cr₂S₃ by DFT methods.
- ³⁹S. Klotz, J. C. Chervin, P. Munsch, and G. L. Marchand, *J. Phys. D: Appl. Phys.* **42**, 075413 (2009).
- ⁴⁰D. Errandonea, Y. Meng, M. Somayazulu, and D. Häusermann, *Physica B* **355**, 116 (2005).
- ⁴¹Y. Shen, R. S. Kumar, M. Pravica, and M. F. Nicol, *Rev. Sci. Instrum.* **75**, 4450 (2004).
- ⁴²F. J. Manjón and D. Errandonea, *Phys. Status Solidi B* **246**, 9 (2009).
- ⁴³R. de Jonge, T. J. A. Popma, G. A. Wiegers, and F. Jellinek, *J. Solid State Chem.* **2**, 188 (1970).
- ⁴⁴R. Lelieveld and D. J. W. Ijdo, *Acta Crystallogr. B* **36**, 2223 (1980).
- ⁴⁵F. Birch, *Phys. Rev.* **71**, 809 (1947).
- ⁴⁶R. J. Angel, M. Alvaro, and J. Gonzalez-Platas, *Z. Kristallogr.* **229**, 405 (2014).
- ⁴⁷D. Errandonea, A. Muñoz, and J. Gonzalez-Platas, *J. Appl. Phys.* **115**, 216101 (2014).
- ⁴⁸R. Mittal *et al.*, “Phonon softening and pressure-induced phase transitions in quartz structured compound, FePO₄,” preprint [arXiv:0903.1550](https://arxiv.org/abs/0903.1550) (2009).
- ⁴⁹C. J. Hearn, *J. Phys. C* **5**, 1317 (1972).
- ⁵⁰Z. G. Wu and E. C. Ronald, *Phys. Rev. Lett.* **95**, 037601 (2005).